

University of Louisville

ThinkIR: The University of Louisville's Institutional Repository

Electronic Theses and Dissertations

5-2022

Release kinetics of metronidazole from 3D printed silicone scaffolds.

Sydney E. Herold
University of Louisville

Follow this and additional works at: <https://ir.library.louisville.edu/etd>



Part of the [Biomaterials Commons](#), and the [Biomechanics and Biotransport Commons](#)

Recommended Citation

Herold, Sydney E., "Release kinetics of metronidazole from 3D printed silicone scaffolds." (2022).
Electronic Theses and Dissertations. Paper 3921.
<https://doi.org/10.18297/etd/3921>

This Master's Thesis is brought to you for free and open access by ThinkIR: The University of Louisville's Institutional Repository. It has been accepted for inclusion in Electronic Theses and Dissertations by an authorized administrator of ThinkIR: The University of Louisville's Institutional Repository. This title appears here courtesy of the author, who has retained all other copyrights. For more information, please contact thinkir@louisville.edu.

RELEASE KINETICS OF METRONIDAZOLE FROM 3D PRINTED SILICONE
SCAFFOLDS

By

Sydney Elizabeth Herold
B.S., University of Louisville, 2021

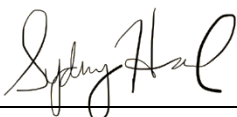
A Thesis
Submitted to the Faculty of the
University of Louisville
J.B. Speed School of Engineering
as Partial Fulfillment of the Requirements
for the Professional Degree

MASTER OF ENGINEERING

Department of Bioengineering

May 2022


RELEASE KINETICS OF METRONIDAZOLE FROM 3D PRINTED SILICONE
SCAFFOLDS

Submitted by:  _____
Sydney Elizabeth Herold

A Thesis Approved on

April 4, 2022

by the following Reading and Examination Committee:



Dr. Jill Steinbach-Rankins, Thesis Chair



Dr. Hermann Frieboes, Committee Member



Dr. Nihat Altıparmak, Committee Member

ACKNOWLEDGEMENTS

I would like to thank my Thesis Chair, Dr. Jill Steinbach-Rankins, for her guidance and unwavering support as I pursued my Master's degree. I would also like to thank the other committee members, Dr. Hermann Frieboes and Dr. Nihat Altiparmak, for their assistance in completing my Thesis. Additionally, I would like to thank each member of the Steinbach-Rankins Lab. It was a joy to work with and learn from everyone throughout the past year. Lastly, I would like to express my thanks to my family for their support throughout my undergraduate and graduate career. I could always count on them to keep my spirits high and without them, I would not be where I am today.

ABSTRACT

RELEASE KINETICS OF METRONIDAZOLE FROM 3D PRINTED SILICONE SCAFFOLDS

Sydney Herold

April 4, 2022

Sustained local administration of active agents has been proposed to cure bacterial vaginosis in the female reproductive tract and restore the resident bacterial fauna. Bioprinting has shown promise for the development of systems for local agent delivery. In contrast to oral ingestion, agent release kinetics can be fine-tuned by bioprinting specialized scaffold designs tailored for particular treatments while enhancing dosage effectiveness via localized sustained release. It has been challenging to establish scaffold properties for sustained release as a function of fabrication parameters. Towards this goal, we evaluate 3D printed scaffold formulation and feasibility to sustain release of metronidazole, a representative antibiotic. Silicone scaffolds were printed in a cylindrical design and cured using three different conditions relevant to potential future incorporation of temperature-sensitive labile biologics. Scaffold A was cured 4 hr at 50°C followed by 72 hr at 4°C, while Scaffold B was cured 4 hr at 50°C followed by 24 hr desiccation at room temperature and Scaffold C was cured 24 hr at 50°C. Drug release and compressive strength were monitored for 14 d in simulated vaginal fluid to assess long-term effects of fabrication conditions on release kinetics and mechanical integrity. Release profiles were

fitted to previous kinetic models to differentiate potential release mechanisms. Scaffold A released 54.1% of drug over 14 d compared to 40.8% for Scaffold B and 33.7% for Scaffold C. Of six models evaluated, the Higuchi, Korsmeyer-Peppas, and Peppas-Sahlin models best described the release, indicating similarity to release from insoluble or polymeric matrices. All scaffolds were axially and radially compressed to determine compressive strength and compressive Young's modulus. For all metronidazole-containing scaffolds, similar axial and radial compression was observed between post-cure and 24 hr and 14 d groups. We conclude that 3D printed silicone scaffolds can provide sustained metronidazole release over 14 d, with release kinetics and compressive strength tuned by the fabrication parameters.

NOMENCLATURE

3D	3-Dimensional
BV	Bacterial vaginosis
EVAc	Ethylene-vinyl acetate copolymer
FTR	Female reproductive tract
HIV	Human immunodeficiency virus
IVR	Intra-vaginal ring
STI	Sexually transmitted disease
SVF	Simulated vaginal fluid

TABLE OF CONTENTS

Approval Page.....	iii
Acknowledgements.....	iv
Abstract.....	v
Nomenclature.....	vii
List of Tables.....	x
List of Figures.....	xi
Introduction.....	1
Materials and Methods.....	6
Synthesis of 3D Printed Silicone Scaffolds Containing Metronidazole.....	6
Synthesis of Printable Silicone Ink.....	6
Printing Scaffolds.....	7
Curing and Storage Time/Conditions.....	7
Metronidazole Incorporation.....	8
Drug Release Studies.....	8
Mechanism of Drug Release.....	9
Mechanical Testing.....	11
Statistics.....	12
Results.....	13
Drug Release from 3D Printed Silicone Scaffolds.....	13
Kinetic Models of Drug Release.....	14
Mechanical Properties.....	15
Compression.....	15
Axial Compression.....	15
Radial Compression.....	17
Young's Modulus.....	19

Axial Young's Modulus.....	19
Radial Young's Modulus.....	20
Discussion.....	22
References.....	29
Appendix.....	33
Curriculum Vita.....	42

LIST OF TABLES

TABLE	PAGE
1. Model Correlation Values.....	41

LIST OF FIGURES

FIGURE	PAGE
1. Image of the tested 3D-printed scaffold design.....	33
2. Short-term and Long-term metronidazole release curves.....	34
3. Scaffold A metronidazole release fitted to kinetic models.....	35
4. Scaffold B metronidazole release fitted to kinetic models.....	36
5. Scaffold C metronidazole release fitted to kinetic models.....	37
6. Axial compression of blank and metronidazole containing scaffolds.....	38
7. Radial compression of blank and metronidazole containing scaffolds.....	39
8. Young's modulus of blank and metronidazole containing scaffolds.....	40

I. INTRODUCTION

Bacterial vaginosis (BV) is a common vaginal infection diagnosed in approximately 1 in 3 women of reproductive age in the U.S.¹. BV results from a loss of healthy, lactic acid producing, lactobacilli and an increase in facultative and anaerobic bacteria in the vagina¹⁻³. One of the prominent anaerobes associated with BV is *Gardnerella vaginalis*, a pH-sensitive bacterium that grows well in slightly acidic pH but is unable to grow in the low pH of the healthy female reproductive tract (pH 4.5)^{3,4}. Symptoms of BV include discoloration and malodorous discharge, vaginal itching and burning^{2,5}. However, more severe long-term afflictions can present, resulting in a variety of pregnancy complications, preterm delivery, and an increased susceptibility to HIV and other sexually transmitted infections (STIs)¹.

The current standard of treatment for women diagnosed with BV is a 5d to 7d oral or topical regimen with an antibiotic such as metronidazole, with twice daily oral regimens or once-daily intravaginal gel application for 5d to 7 d^{6,7}. Topical administration has been shown to be advantageous as it avoids the adverse effects related to oral administration while allowing localized drug release directly at the site of infection. Moreover, a variety of dosage forms, including vaginal gels, suppositories, nanoparticle-based systems, and

intravaginal rings (IVRs) have been used to administer antibiotics and other active agents in efforts to topically eliminate a variety of intravaginal infections⁸⁻¹⁴. Yet, with the exception of IVRs, these dosage forms act transiently and necessitate frequent daily administrations to exert therapeutic effect. Furthermore, the leakage and associated messiness associated with current dosage forms can result in a lack of user adherence and compliance, which in turn can promote antibiotic-resistance and non-specific elimination of commensal bacteria, ultimately leading to recurrent infections. As an alternative strategy, probiotics have demonstrated success in restoring vaginal flora and reestablishing a healthy acidic pH making the vaginal environment less hospitable to the colonization of pathogens such as *G. vaginalis*. However, much like antibiotic dosage forms, there are a dearth of topical probiotic or combination dosage forms that provide sustained or phased co-delivery of one or more active agents to reduce recurrent bacterial (and viral) infections.

One of the few dosage forms that has demonstrated success in attaining long-term intravaginal delivery is intravaginal rings. A variety of polymers including silicone, polyurethanes, and ethylene vinyl acetate (EVAc) have been used to facilitate the release of hydrophobic molecules, such as hormones, and more recently antibiotics, such as metronidazole, for intravaginal applications^{15,16}. Silicone, in particular, has been shown to have exceptional biocompatibility, low surface tension for uniform drug distribution, as well as biodurability in low pH environments¹⁷. However, IVR fabrication typically relies on molding techniques that can be susceptible to deformation and contamination, in addition to harsh solvents, temperatures, and multistep fabrications that may be less amenable to the inclusion of more labile biologic agents¹⁸.

A proposed solution to improve upon the duration of administration, multi-therapeutic compatibility of manufacturing, and throughput of the fabrication process, is to utilize extrusion-based 3D printing. Extrusion-based 3D printing, in combination with computer aided design, can be used to fabricate architectures with discrete compartments to facilitate the release of different active agents from sequentially-printed layers¹⁹. These features enable the fabrication of simple and complex architectures that can provide personalized dosing with sustained release and increased bioavailability of drug at a localized site. One notable example is the polypill, PolycapTM, which is commercially available to treat hypertension and cardiovascular disease^{20,21}. Through the development of the polypill, 3D printing has shown promise in producing consistent complex geometric designs with multiple drug formulations. While 3D printing has been utilized for a few vaginal applications²²⁻²⁷, it has not been extensively studied for vaginal drug delivery.

While 3D printing has the potential to provide a novel and efficacious alternative dosage form for reproductive health, a variety of factors including material properties, scaffold architecture, and post-print processing can affect the dosage form design and resulting release properties. Design optimization can require numerous experimental iterations depending on the critical parameters of interest. Complementing formulation development with mathematical modeling enables the knowledge of physical parameters, such as drug diffusion coefficients and polymer relaxation coefficients, to be combined with mathematical equations representing a given system, to help establish, predict, and validate parameters integral to achieving design criteria. In particular, mathematical modeling may be useful in establishing key outcomes, such as release kinetics, mechanical

integrity, and degradation as a function of the post-processing conditions of new 3D printed dosage forms.

In this study, one of the key considerations to the 3D printed scaffold design was the ability to prolong metronidazole release for durations of one week or longer. Additionally, since we seek to design future scaffolds to co-deliver other active agents, including more labile biologics, the duration and temperature of post-print processing were primary parameters of interest in enabling sustained release. With this long-term goal in mind, we considered the effect of scaffold curing temperature and time on metronidazole release.

We fabricated three different 3D printed silicone scaffold formulations, which varied in their post-print curing conditions, and evaluated *in vitro* drug release in simulated vaginal fluid (SVF). One formulation included a post-print cure for 4 hr at 50°C, followed by incubation for 72 hr at 4°C to enhance the mechanical integrity of the scaffold. An additional formulation included a post-print cure for 4 hr at 50°C followed by incubation at room temperature (20°C) for 24 hr. Similar to the first formulation, these curing conditions aimed to enhance the mechanical integrity of the scaffold while minimizing the scaffold time spent at room temperature. Metronidazole-containing scaffolds cured for 24 hr at 50°C (Scaffold C) had the highest compressive strength immediately post cure, however following 14 d immersion in SVF scaffolds cured for 4 hr at 50°C followed by 72 hr at 4°C (Scaffold A) had the highest compressive strength.

In parallel, we utilized mathematical modeling to evaluate the impact of post-print curing on antibiotic release kinetics. Potential mechanisms of drug release were assessed via established kinetic models, including zero order, first order, Higuchi, Korsmeyer-

Peppas, Hixson-Crowell, and Peppas-Sahlin²⁸. The modeling was employed to provide evidence that the formulated scaffolds release metronidazole via diffusion-controlled release from silicone, in order to validate our drug delivery system as a viable treatment for sustained intravaginal delivery.

II. MATERIALS AND METHODS

A. Materials

A mixture of Part A: vinyl-terminated polydimethylsiloxane (70%, PDMS) and vinyl, methyl-modified silica (30%) and Part B: trimethylsiloxane-terminated methylhydrosiloxane-dimethylsiloxane copolymer, were purchased from Allevi, Inc. (Philadelphia, PA). Dimethyl sulfoxide (DMSO, Fischer Scientific, B231-1), and Metronidazole (Sigma Aldrich, M3761-5G) were used to formulate the bioink. Simulated vaginal fluid (SVF) was prepared as mentioned in^{29,30}.

B. Synthesis of 3D Printed Silicone Scaffolds Containing Metronidazole

1. Synthesis of Printable Silicone Ink

3D printed scaffolds were formulated from a mixture of Part A:Part B and metronidazole. Briefly, metronidazole (55 mg) was weighed, ground to a fine powder with a mortar and pestle, and added to a microcentrifuge tube containing 60 μ L DMSO. The silicone consisting of 1.0 g:0.1 g of Part A:Part B PDMS, respectively, was then added to

the microcentrifuge tube and vortexed to ensure homogeneity. The ink was then vigorously mixed with a spatula for a minimum of 5 minutes.

2. Printing Scaffolds

A 1 mL aliquot of metronidazole “ink” was loaded into a 5 mL syringe and placed into the CORE head of the Allevi 3 Bioprinter. A customized Stereolithography (STL) file was created in the form of a cylindrical capsule. The capsule dimensions were sized for a mouse model of BV: 5 mm in height, 4 mm in diameter, with a shell thickness of 0.5 mm. The Allevi 3 Bioprinter was used to 3D print all scaffolds. The extrusion pressure was set at 100 psi, the CORE head of the extruder was set at 30°C, and the extrusion flow rate was set at 5 mm/sec. The layer height for printing was set at 0.2 mm, the infill distance was fixed at 0.35 mm with zig-zag infill type, and a 23G needle gauge was used for extruding the formulated bioink. Scaffolds were printed in a petri dish using the STL file as a printing template and were then subjected to one of three different post-print curing conditions.

3. Curing and Storage Time/Conditions

Three different 3D printed silicone scaffold formulations were fabricated, with variations in their post-print curing conditions. Scaffold A was cured in an oven at 50°C for 4 hr, followed by incubation at 4°C for 72 hr. The curing conditions established for this scaffold consider the potential of future biologic inclusion by attempting to minimize high temperature exposure which can lead to biologic inactivation^{31,32}. Scaffold B was cured at 50°C for 4 hr, followed by incubation at 20°C for 24 hr which sought to improve the mechanical integrity of the scaffold while minimizing duration of exposure to temperatures

higher than 50°C. Scaffold C was cured at 50°C for 24 hr to provide the most mechanically sound structure, per the conventional Allevi printing protocol.

4. Metronidazole Incorporation

A metronidazole concentration of 50 µg/mg was selected for initial loading as this concentration was found to eliminate anaerobes including, *G. vaginalis*, *Prevotella* species, and *Bacteroides* species based upon their MIC₅₀ values (< 8 µg/mL), and the susceptibility breakpoint concentration for metronidazole defined by the Clinical and Laboratory Standards Institute (CLSI). In comparison, commensal lactobacilli have a MIC₅₀ >128 µg/ml for metronidazole, enabling some level of evaluation with treatment³³⁻³⁹. The theoretical loading (µg) of each scaffold was calculated based on the scaffold weight and the concentration of metronidazole in the silicone ink (Eq. 1).

$$\textit{Theoretical Loading } (\mu\text{g}) = \textit{Scaffold Mass } (\text{mg}) * \textit{Drug Concentration } (\mu\text{g}/\text{mg}) \quad (1)$$

C. Drug Release Studies

In vitro drug release was evaluated in SVF. The prepared metronidazole-containing silicone scaffolds were submerged in 5 mL of SVF (pH 4.2) and incubated at 37°C to mimic physiological temperature. Metronidazole release was evaluated at 2, 4, 8 hr, and after 1, 2, 3, 4, 5, 6, 7, 8, 9, 10, and 14 d. At established times, SVF was removed from the 5 mL tubes, scaffolds were washed with 1x PBS, and fresh SVF was added. The amount of metronidazole in each eluate sample was determined by reading absorbance (320 nm, Gen 5 app, BioTek Synergy H1 Microplate Reader) and correlating with a metronidazole

standard curve. The cumulative release of metronidazole was calculated as the μg of metronidazole released per mg scaffold and as the % total loaded shown in Eq. 2.

$$\% \text{ Cumulative Drug Release} = \frac{[Drug]_t}{[Drug]_{total}} * 100 \quad (2)$$

where $[Drug]_t$ refers to the amount of drug release at time t and $[Drug]_{total}$ refers to the total amount of drug loaded into the scaffold.

D. Mechanism of Drug Release

To assess the mechanism of drug release, representative kinetic models were used to analyze the release data based on previous modeling efforts that incorporated metronidazole. The zero order kinetic model describes drug release independent of drug concentration in solution (Eq. 3)⁴⁰,

$$Q_t = Q_0 + kt \quad (3)$$

where Q_t is the amount of drug dissolved in time t , Q_0 is the initial amount of drug in solution, and k is the zero order rate constant. The first order kinetic model describes drug release dependent on drug concentration (Eq. 4)⁴⁰,

$$\log C = \log C_0 - \frac{kt}{2.303} \quad (4)$$

where C is drug concentration at time t , C_0 is initial drug concentration, and k is the first order rate constant. The simplified Higuchi model describes drug release from polymeric systems, where dissolution is the main method of drug transfer (Eq. 5)⁴¹.

$$\frac{M_t}{M_\infty} = k\sqrt{t} \quad (5)$$

where M_t/M_∞ is the cumulative amount of drug released at time t , and k is the Higuchi rate constant, also known as the diffusion coefficient. The Korsmeyer-Peppas model describes drug release from polymeric matrices (Eq. 6)⁴⁰.

$$\frac{M_t}{M_\infty} = k't^n \quad (6)$$

where M_t/M_∞ is the cumulative drug release at time t , k' is the drug release coefficient, and n describes a mechanism of diffusion. The Hixson Crowell cube root model utilizes the proportionality of a particle's area to its volume to describe drug release (Eq. 7)⁴²,

$$W_0^{1/3} - W_t^{1/3} = kt \quad (7)$$

where W_0 is the initial amount of drug, W_t is the remaining amount of drug at time t , and k is the rate rate constant. The Peppas-Sahlin model accounts for the effects of Fickian diffusion and polymer chain relaxation when describing drug release (Eq. 8)⁴³,

$$\frac{M_t}{M_\infty} = k_d t^m + k_r t^{2m} \quad (8)$$

where M_t/M_∞ is the cumulative drug release at time t , k_d is the kinetic constant associated with Fickian diffusion, k_r is the kinetic constant associated with polymer chain relaxation, and m is the purely Fickian diffusion exponent⁴³.

Each model's adequacy was evaluated using MATLAB Curve Fitting Toolbox. Once the parameters were obtained, graphs were constructed using Microsoft Excel. All models were obtained by plotting cumulative percent drug release against time and using the Custom Equation option to fit the model to the data.

E. Mechanical Testing

The compressive strength and Young's modulus of the scaffolds were evaluated as a function of curing condition. Blank silicone and metronidazole-containing silicone scaffolds were assessed after curing with the following conditions: 50°C for 4 hr, followed by incubation at 4°C for 72 hr; 50°C for 4 hr, followed by incubation at 20°C for 24 hr; and 50°C for 24 hr (Scaffold A, B, and C, respectively). Scaffolds were assessed immediately post-cure, and after 24 hr or 14 d in SVF.

Axial and radial compression was measured using the Instron 5569 testing system, and data were extrapolated using Instron Bluehill software (Norwood, MA). Compression test parameters were selected to represent the range with which commercial IVRs have been tested⁴⁴⁻⁴⁶. A 5 kN load cell was used, and the applied force was varied between 0.6 and 1.6 N. The transducer was lowered to the scaffold surface prior to the test and transducer displacement was set to 1 mm with a displacement rate of 1 mm/min. These

configurations are equivalent to 20% or 25% compression in the axial and radial directions, respectively.

F. Statistics

Drug release and compression measurements were performed using a minimum of $n=3$ samples per run. Error bars denote standard deviation (SD), and results are reported as the mean \pm SD. The software Minitab was used to statistically analyze metronidazole release from 3D printed silicone scaffolds. A Grubbs' test was utilized to determine the presence of outliers ($p \leq 0.05$). Statistical significance between the final release values, as a function of curing condition, was verified using a paired t-test ($p \leq 0.05$). One-way ANOVA was used to evaluate the mechanical testing results and determine the statistical significance between scaffolds.

III. RESULTS

A. Drug Release from 3D Printed Silicone Scaffolds

The tested 3D-printed scaffold design is shown in **Figure 1**.

Metronidazole was completely dissolved in silicone during the fabrication of the printable silicone ink to evaluate drug release kinetics. The cumulative release of metronidazole is shown as a function of percent of total loading (**Figure 2**). Overall, the 3D printed silicone scaffolds showed a steady release of metronidazole within the first 6 hr, following a common trend observed with small molecules^{6,28,47,48}. Post-print curing condition proved to have an effect on cumulative release. Scaffold A showed the highest metronidazole release, with $15.8 \pm 2.4\%$ release occurring in the first 24 hr, followed by a steady increase to $54.1 \pm 2.9\%$ after 14 d. Scaffold B showed intermediate levels of release, with $10.2 \pm 0.8\%$ of drug released during the first 24 hr and $40.8 \pm 4.1\%$ after 14 d. Scaffold C showed the least overall release with $8.7 \pm 2.4\%$ release over the first 24 hr and only $33.7 \pm 5.1\%$ release after 14 d. For short-term (24 hr) and long-term (14 d) drug release, statistical significance ($p \leq 0.05$) was observed between Scaffolds A and B and between Scaffolds A and C, however release from Scaffolds B and C were not statistically

significant. The post-print curing condition of Scaffold A (4 hr at 50°C followed by 72 hr at 4°C) provided enough mechanical integrity to extend drug release over 14 d. Accordingly, this formulation may be a promising curing condition to use for eventual inclusion of more labile biologics.

B. Kinetic Models of Drug Release

Previously developed mathematical kinetic models are useful to evaluate potential mechanisms of drug release, and they were applied here to study metronidazole release from the 3D printed silicone scaffolds. For each scaffold formulation, *in vitro* release curves (**Figure 2**) were fitted to various representative kinetic models to describe potential mechanisms of release (**Figures 3-5**).

The resulting correlation values and rate constants for all models are summarized in **Table 1**.

Each model exhibited similar R^2 values across the three different post-print curing conditions; therefore, the most appropriate condition can be selected without it affecting the mechanism of metronidazole release. The Higuchi, Korsmeyer-Peppas, and Peppas-Sahlin models best described the release of metronidazole from the 3D printed silicone scaffolds. The Higuchi model had an $R^2=0.9918$ (Scaffold A), $R^2=0.9955$ (Scaffold B), and $R^2=0.9954$ (Scaffold C). The Korsmeyer-Peppas model had an $R^2=0.9931$ (Scaffold A), $R^2=0.9959$ (Scaffold B), and $R^2=0.9958$ (Scaffold C). Lastly, the Peppas-Sahlin model had an $R^2=0.9990$ (Scaffold A), $R^2=0.9990$ (Scaffold B), and $R^2=0.9980$ (Scaffold C). This indicates that the release of metronidazole, a hydrophobic drug, from silicone, a hydrophobic polymer, is best modeled similar to drug release from an insoluble matrix or

from a polymeric matrix^{6,48}. The zero order model showed the lowest correlation to experimental metronidazole release with an $R^2=0.6862$ (Scaffold A), $R^2=0.7667$ (Scaffold B), and $R^2=0.7699$ (Scaffold C), indicating the release of metronidazole from 3D printed silicone scaffolds is not independent of drug concentration in solution^{40,49}. This is confirmed by the first order model showing significantly improved correlation compared to the zero order model for all post-print curing conditions, although not quite reaching the performance of the best three models.

C. Mechanical Properties

1. Compression

The load required to compress each scaffold was evaluated as a function of scaffold curing conditions immediately post-cure, and after 24 hr and 14 d in SVF. All scaffolds were compressed by 20% of their height and 25% of their diameter, in the axial and radial directions, respectively.

a. Axial Compression. First the axial compression of blank and metronidazole-containing scaffolds was assessed (**Figure 6**). For blank silicone scaffolds, the load required to axially compress scaffolds immediately post-cure and after 24 hr in SVF (**Figure 6A-C**) was lower after curing for 4 hr at 50°C (Scaffolds A and B) compared to scaffolds cured for 24 hr at 50°C (Scaffold C, $p \leq 0.0001$). However, all blank scaffolds exhibited similar axial compression following 14 d immersion in SVF ($p > 0.05$).

Within each blank scaffold group (A, B, or C), the load required to achieve axial compression was similar between post-cure and 24 hr cure groups ($p > 0.05$); however,

increased between post-cure and 14 d groups (Scaffolds A, B, C: $p \leq 0.01$; $p \leq 0.0001$; $p \leq 0.05$) (**Figure 6A-C**). Additionally, scaffolds cured for 4 hr at 50°C (Scaffolds A and B) showed increased loads required to compress scaffolds immersed for 24 hr and 14 d (Scaffolds A, B: $p \leq 0.01$; $p \leq 0.001$), while scaffolds cured for 24 hr at 50°C (Scaffold C) required similar loading to achieve compression ($p > 0.05$).

For metronidazole-containing scaffolds, the load required to axially compress scaffolds immediately post-cure was lower after curing for 4 hr at 50°C (Scaffolds A and B) compared to scaffolds cured for 24 hr at 50°C (Scaffold C; Scaffolds A, B: $p \leq 0.05$; $p \leq 0.01$). All metronidazole-containing scaffolds exhibited similar axial compression following 24 hr immersion in SVF ($p > 0.05$). Finally, the load required to axially compress scaffolds after 14 d immersion in SVF was largest for Scaffold A (cured for 4 hr at 50°C followed by 72 hr at 4°C) compared to Scaffolds B and C (Scaffolds B, C: $p \leq 0.01$; $p \leq 0.001$).

Within each metronidazole-containing scaffold group and similar to blank scaffolds, the loads required to axially compress all metronidazole-containing post-cure and 24 hr scaffold groups were similar ($p > 0.05$) (**Figure 6D-F**). The axial compression load only increased between post-cure and 14 d groups for scaffolds cured for 4 hr at 50°C (Scaffolds A and B, $p \leq 0.0001$), while axial compression was similar between the post-cure and 14 d groups cured for 24 hr at 50°C (Scaffold C, $p > 0.05$). Additionally, the axial compression load increased between 24 hr and 14 d groups for all metronidazole-containing scaffolds (Scaffolds A and B, $p \leq 0.0001$; Scaffold C, $p \leq 0.01$).

In comparing the load required to axially compress blank, relative to metronidazole-containing scaffolds, significant effects were observed. Overall, and based on the average of all immersion conditions for each scaffold type (A, B, or C), the load required to axially compress blank scaffolds was approximately 8-fold, 12-fold, and 18-fold higher for Scaffolds A, B, and C, respectively, than that needed for similar compression of metronidazole-containing (A, B, or C) scaffolds. These results suggest that metronidazole incorporation at the specified concentration may weaken the scaffolds under axial compression.

b. Radial Compression. Following axial compression, all scaffolds were compressed in the radial direction to account for additional forces the scaffolds may experience in the vaginal environment. For blank silicone scaffolds, the loads required to radially compress scaffolds immediately post-cure and after 24 hr in SVF (**Figure 7A-C**) were lower after curing for 4 hr at 50°C (Scaffolds A and B; $p \leq 0.01$ and $p \leq 0.0001$), relative to scaffolds cured for 24 hr at 50°C (Scaffold C). However, similar to that observed in axial compression, all blank scaffolds exhibited similar radial compression following 14 d in SVF ($p > 0.05$).

Within each blank scaffold group (A, B, or C), Scaffolds A and B showed increased loads needed to achieve radial compression for the 14 d in SVF group, relative to scaffolds assessed post-cure (Scaffolds A, B: $p \leq 0.05$; $p \leq 0.001$) and after 24 hr immersion in SVF (Scaffolds A, B: $p \leq 0.05$; $p \leq 0.001$), while demonstrating similar compression between the immediate post-cure and 24 hr in SVF groups (**Figure 7A-B**, $p > 0.05$). Within the blank Scaffold C group (cured for 24 hr at 50°C) radial compression was similar between post-cure, 24 hr, and 14 d groups (**Figure 7C**, $p > 0.05$).

For metronidazole-containing scaffolds, the load required to radially compress scaffolds immediately post-cure was lower after curing for 4 hr at 50°C (Scaffolds A and B) compared to scaffolds cured for 24 hr at 50°C (Scaffold C, $p \leq 0.01$). All metronidazole-containing scaffolds exhibited similar radial compression following 24 hr immersion in SVF ($p > 0.05$). Finally, the load required to axially compress scaffolds after 14 d immersion in SVF was highest for Scaffold A (cured for 4 hr at 50°C followed by 72 hr at 4°C) compared to Scaffolds B ($p \leq 0.001$) and C (**Figure 7D-F**, $p \leq 0.0001$).

Within each metronidazole-containing scaffold group, Scaffold A showed a significant increase in load required to radially compress the 14 d in SVF, relative to both the immediate post-cure group and 24 hr in SVF group (**Figure 7D**, $p \leq 0.0001$). Additionally, Scaffold B showed a significant increase in the load required to radially compress the 24 hr and 14 d in SVF, relative to the immediate post-cure group (**Figure 7E**, $p \leq 0.01$). In comparison, radial compression was similar for Scaffold C (cured for 4 hr at 50°C), between post-cure and 14 d groups ($p > 0.05$) and increased between 24 hr and 14 d groups (**Figure 7F**, $p \leq 0.05$).

Last and similar to axial compression observations, the load required to radially compress blank scaffolds was approximately 21-fold, 25-fold, and 30-fold (for Scaffolds A, B, and C) higher than that needed for similar compression of metronidazole-containing scaffolds. These results suggest that metronidazole incorporation at the specified concentration may weaken the scaffolds under radial compression. Additionally, both blank and metronidazole-containing silicone scaffolds exhibited lower compressive strength in the radial direction, relative to the axial direction.

2. Young's Modulus

Using compressive stress and strain measurements, the axial and radial Young's modulus were obtained as a function of curing conditions (Scaffold A, B, or C) immediately post-cure, and after 24 hr and 14 d in SVF (**Figure 8**).

a. Axial Young's Modulus. Within each blank scaffold group (Scaffolds A, B, or C), the axial Young's modulus was similar between post-cure and 24 hr groups ($p > 0.05$); however, increased between the post-cure and 14 d groups (**Figure 8A**) (Scaffolds A, $p \leq 0.01$; B, $p \leq 0.0001$; C, $p \leq 0.05$). Additionally, for scaffolds cured for 4 hr at 50°C (Scaffolds A and B), the axial Young's modulus increased between 24 hr and 14 d groups (Scaffold A, B: $p \leq 0.01$; Scaffold B, $p \leq 0.001$).

As a function of immersion duration (analysis post-cure, 24 hr SVF, or 14 d SVF), the axial Young's modulus significantly increased after curing for 24 hr at 50°C (Scaffold C) for the post-cure (Scaffolds A, B: $p \leq 0.001$; $p \leq 0.01$) and 24 hr conditions (Scaffolds A, B: $p \leq 0.0001$; $p \leq 0.01$), relative to a shorter curing duration of 4 hr at 50°C (Scaffolds A and B). In comparison, for the 14 d immersion samples, the axial Young's modulus was similar across blank scaffolds (A, B, and C, $p > 0.05$).

For metronidazole-containing scaffolds, the axial Young's modulus (**Figure 8B**) increased between post-cure and 24 hr in SVF groups for Scaffold B (cured for 4 hr at 50°C followed by 24 hr desiccation at room temperature, $p \leq 0.05$), while remaining similar between post-cure and 24 hr groups for Scaffold A (cured for 4 hr at 50°C followed by 72 hr at 4°C) and Scaffold C (cured for 24 hr at 50°C). Additionally, the axial Young's modulus increased for all metronidazole-containing scaffolds between post-cure and 14 d

groups (Scaffolds A, B, C: $p \leq 0.0001$; $p \leq 0.0001$; $p \leq 0.05$) and between 24 hr and 14 d groups (Scaffolds A, B, C: $p \leq 0.0001$; $p \leq 0.0001$; $p \leq 0.001$).

As a function of immersion duration, the Young's modulus of the metronidazole-containing scaffolds assessed immediately post-cure and cured for 24 hr at 50°C (Scaffold C) was higher than post-cure assessed scaffolds that were cured for only 4 hr at 50°C (Scaffolds A, B: $p \leq 0.01$; $p \leq 0.001$). For the 24 hr SVF immersion group, all metronidazole-containing scaffolds had similar axial Young's modulus ($p > 0.05$). Finally, for the 14 d group, Scaffold A (cured for 4 hr at 50°C followed by 72 hr at 4°C) had a higher axial Young's modulus compared to Scaffolds B (cured for 4 hr at 50°C followed by 24 hr desiccation at room temperature) and C (cured for 24 hr at 50°C) ($p \leq 0.0001$).

b. Radial Young's Modulus. Similar to axial observations, the radial Young's modulus was evaluated as a function of curing conditions immediately post-cure, and after 24 hr and 14 d in SVF (**Figure 8C-D**). Within each blank scaffold group (Scaffolds A, B, or C), only scaffolds cured for 24 hr at 50°C (Scaffold C) showed an increase in Young's modulus between post-cure and 24 hr conditions ($p \leq 0.01$). Additionally for each blank scaffold group (A, B, and C), the radial Young's modulus increased between post-cure and 14 d conditions (Scaffolds A, B, C: $p \leq 0.01$; $p \leq 0.0001$; $p \leq 0.01$), while scaffolds cured for 4 hr at 50°C (Scaffolds A and B) showed additional increases between 24 hr and 14 d groups (Scaffold A, B: $p \leq 0.05$; $p \leq 0.001$).

As a function of immersion duration (analysis post-cure, 24 hr SVF, or 14 d SVF), the radial Young's modulus of blank scaffolds remained similar across post-cure groups (**Figure 8C**, $p > 0.05$). For the 24 hr in SVF group, scaffolds cured for 24 hr at 50°C

(Scaffold C) had a higher radial Young's modulus compared to scaffolds cured for 4 hr at 50°C (Scaffolds A, B: $p \leq 0.0001$; $p \leq 0.001$). All scaffolds immersed in SVF for 14 d had similar Young's modulus.

For metronidazole-containing scaffolds, only Scaffold B (cured for 4 hr at 50°C followed by 24 hr desiccation at room temperature) showed an increase in radial Young's modulus (**Figure 8D**) between post-cure and 24 hr groups ($p \leq 0.05$). However, metronidazole-containing scaffolds cured for 4 hr at 50°C (Scaffolds A and B) increased in radial Young's modulus (**Figure 8D**) between post-cure and 14 d conditions (Scaffolds A, B: $p \leq 0.0001$; $p \leq 0.01$), and between 24 hr and 14 d conditions for Scaffold A ($p \leq 0.0001$). In comparison, scaffolds cured for 24 hr at 50°C (Scaffold C) showed similar Young's modulus across immersion conditions ($p > 0.05$).

As a function of immersion duration, the radial Young's modulus of metronidazole-containing scaffolds cured for 24 hr at 50°C (Scaffold C) and assessed immediately post-cure had a higher radial Young's modulus than scaffolds cured for 4 hr at 50°C (Scaffolds A and B, $p \leq 0.01$). For metronidazole-containing scaffolds assessed after 24 hr immersion in SVF, all had similar radial Young's modulus ($p > 0.05$). Finally, for scaffolds assessed after 14 d immersion in SVF, Scaffold A (cured for 4 hr at 50°C followed by 72 hr at 50°C) showed a significant increase in radial Young's modulus compared to Scaffolds B (cured for 4 hr at 50°C followed by 24 hr desiccation at room temperature) and C (cured for 24 hr at 50°C) ($p \leq 0.0001$).

IV. DISCUSSION

In this study, metronidazole-containing 3D printed silicone scaffolds were fabricated to evaluate sustained release kinetics for the potential treatment of BV. Metronidazole, as a model hydrophobic active agent, was incorporated into silicone by dissolving in DMSO and physically mixing⁵⁰. The drug-incorporated ink was loaded into a syringe and 3D printed using previously mentioned printing parameters. Three different post-print curing conditions were evaluated to enhance mechanical integrity prior to immersing each scaffold in SVF for drug release studies and fitting of release profiles to representative kinetic models.

The release kinetics of metronidazole have been studied previously, using a wide variety of computational models, materials, dosage forms. In one study, metronidazole was incorporated into HPMC, psyllium, and Carbopol to fabricate a floating dosage form to treat peptic ulcer disease²⁸. Metronidazole release was modeled using similar models to this study, such as zero-order kinetic, first-order kinetic, Higuchi, Hixson-Crowell, Power law, and the Weibull model. Metronidazole release from the tablet was best modeled by the power law, as the release is dependent on Fickian diffusion and polymer relaxation. In another study, metronidazole was incorporated into mesostructured silica-based materials to treat bone disease⁶. Metronidazole release was found to differ based on the addition of various types of organic groups onto the silica. The drug release was adequately modeled by the Korsmeyer-Peppas model, which indicated diffusion-controlled release.

Metronidazole has also been incorporated into alginate beads with calcium silicate acting as a porous carrier to facilitate release⁵¹. Javadzadeh et al. modeled the release of metronidazole using similar models to this study, and also included linear probability, log probability, and the reciprocal powered time models. The release was shown to be best modeled by the reciprocal powered time, Weibull, and log probability models.

Additionally, the use of silicone as a means of drug delivery has been previously studied and modeled. In one study, ibuprofen and diclofenac were incorporated into a multi-layered silicon matrix system and the release kinetics were modeled using a numerical model⁵². The model parameters included diffusion, effective dissolution rate, and solubility coefficients. Based on support from experimental data, the fabricated numerical model could be used to design controlled drug release multi-layer silicone devices. In another study, dexamethasone was incorporated into silicone and the release was fitted to a previously derived equation⁵³. The model highlighted the impact that system geometry, size, and composition may have on the drug release kinetics.

In this study, while post-print curing condition did not show an effect on the mechanism of metronidazole release from silicone, it proved to have an effect on cumulative release. After 24 hr, Scaffold A showed the greatest percent drug release at 15.8%, followed by Scaffold B at 10.2%, then Scaffold C at 8.7%. After 14 d, Scaffold A released 54.1% of drug, relative to 40.8% for Scaffold B and 33.7% for Scaffold C. Due to the hydrophobicity of metronidazole, none of the scaffolds exhibited substantial burst release within the first 24 hr, in agreement with release profiles observed for metronidazole from other delivery platforms^{10,28}. In congruence with *in vitro* data, metronidazole release from Scaffolds A, B, and C was best modeled by the Higuchi, Korsmeyer-Peppas, and

Peppas-Sahlin kinetic models. All three models have previously been used to adequately describe drug release from polymeric matrices, suggesting the 3D printed silicone scaffolds can be modeled similarly to polymeric matrix systems.

The Higuchi model describes drug release from matrix systems via diffusion-controlled release and relies on the following assumptions: (i) initial drug concentration is much higher than solubility drug concentration, (ii) drug diffusion takes place in one dimension (edge effects are negligible), (iii) drug particles are much smaller than the delivery system, (iv) drug diffusivity is constant, and (v) perfect sink conditions exist in the release environment⁴⁰. The Korsmeyer-Peppas model is a semi-empirical model that utilizes the first 60% of the drug release curve to determine the mechanism of drug release using the value of the release exponent, n ⁴⁰.

For all scaffolds, the release exponent indicated anomalous transport, as the exponents varied between 0.45 and 0.89. This suggested that the mechanism of drug release is a combination of Fickian diffusion and polymer relaxation, which resulted in the release data being fit to the Peppas-Sahlin model⁴³. This semi-empirical model uses two terms to isolate the drug transport attributed to either Fickian diffusion or polymer relaxation. For all scaffolds, k_d was much greater than k_r , indicating that the main mechanism of transport of metronidazole from the silicone scaffolds is Fickian diffusion. Additionally, all scaffolds exhibited a negative k_r , indicating that polymer chain relaxation is insignificant in the release of metronidazole from silicone⁵⁴.

For comparison, we evaluated the Weibull model as an additional candidate to describe metronidazole release from 3D printed scaffolds. The Weibull model is a general empirical equation that has been widely applied to drug release across dosage forms.

However, it is limited in its ability to provide comparisons between *in vivo* and *in vitro* release and lacks many parameters that can be related to dissolution rate⁴². Drug release from all three scaffolds was adequately modeled with $R^2 > 0.98$.

To better understand the relationship between cumulative metronidazole release and curing condition, the compressive strength of the metronidazole-containing scaffolds was evaluated. Compressive strength was evaluated immediately post-cure and following immersion in SVF for 24 hr and 14 d to help evaluate changes in the mechanical integrity of the scaffolds, which may be experienced in the vaginal environment. One of the most striking observations was that both blank and metronidazole-containing scaffolds showed differences in compressive strength between post-cure and 14 d groups, and in particular in both the axial and radial directions for Scaffold A, and to a lesser extent for Scaffold B. In contrast, lesser to negligible differences were observed as a function of immersion duration for Scaffold C. These results support that the shorter duration of or hardening during the curing process may have impacted the mechanical integrity of both blank and metronidazole-containing scaffolds, in particular after longer-term exposure to SVF.

For the metronidazole-containing scaffolds, the most evident increase in compressive strength between the post-cure and 14 d immersion conditions was seen in Scaffold A (cured for 4 hr at 50°C followed by 72 hr at 4°C). In comparison, metronidazole-containing Scaffold B (cured for 4 hr at 50°C followed by 24 hr desiccation at room temperature) had a more attenuated response in the axial and radial directions, while Scaffold C (cured for 24 hr at 50°C) exhibited negligible effect between these immersion conditions. Between post-cure and 14 d immersion in SVF, the load required to axially compress metronidazole-containing Scaffold A increased 6.4-fold, while increasing 6.2-

and 1.5-fold for Scaffolds B and C. Similar trends were observed in the load needed to radially compress metronidazole-containing scaffolds with Scaffold A increased 20-fold following 14 d in SVF, while Scaffolds B and C increased by 5- and 1.3-fold, respectively.

Considering these observations, we suggest that the shorter curing duration of 4 hr may leave scaffolds more mechanically susceptible to compression (e.g., potentially less dense, more porous) than scaffolds cured for 24 hr, perhaps by enabling salts and proteins in SVF to penetrate the scaffolds and impact the mechanical strength. Conversely, depending on structure, metronidazole release may have been more rapid from scaffolds processed with shorter cure durations. Over 14 d immersion in SVF, the metronidazole released from the scaffold may further enable salts in SVF to diffuse into the scaffold leading to an increase in compressive strength. In future work we seek to investigate this relationship more thoroughly to better understand how structural features may impact mechanical integrity after different durations in physiologically relevant environments.

In addition to differences in the load required for compression, all blank and metronidazole-containing scaffolds, demonstrated an increase in Young's modulus between post-cure and 14 d immersion in SVF in the axial direction. Interestingly, Scaffold A showed the greatest cumulative drug release over 14 days, while also exhibiting the largest compressive strength and Young's modulus of all metronidazole-containing scaffolds. After 14 days immersed in SVF, the compressive strength and Young's Modulus (axially and radially) of the scaffolds decreased from Scaffold A to B to C (**Figures 6-8**), while the cumulative drug release decreased from Scaffold A to B to C (**Figure 2**). This trend further supports a potential relationship between drug release and scaffold

curing/structure, particularly over longer durations in a physiologically relevant environment.

Another, and potentially more significant observation was seen by the decrease in compressive strength with the inclusion of metronidazole into the scaffold formulations. The load required to compress blank scaffolds was ~ 8-, 12-, and 18-fold higher (axially) and ~ 21-, 25-, and 30-fold higher (radially) for Scaffolds A, B, and C, respectively, than that needed for similar compression of metronidazole-containing (A, B, or C) scaffolds. These results suggest that metronidazole – at this concentration – may somewhat weaken scaffolds to compression. Yet despite the 8 to 30-fold decrease in compressive strength with the inclusion of metronidazole, the resulting scaffolds have compression strength similar to the EVA-R intravaginal ring⁴⁵ and TFV-HPEU 20 rings⁴⁴, that have compressive loads between 1 and 1.25 N when compressed by 20% of their original outer diameter⁴⁵. Similarly, uniaxial mechanical testing of TFV-HPEU IVRs resulted in a required compressive load less than 1 N to compress rings by 1 mm⁴⁴. Given these comparisons, the mechanical strength of these 3D printed scaffolds suggests that they may be effective for drug release, while having suitable mechanical properties to be inserted and applied for intravaginal applications^{45,55-58}.

Longer term, we propose that a platform that can sustain the delivery of both antibiotics and new biologics may enable an approach to immediately decrease infection and subsequently restore female reproductive health. With further development, the proposed core-shell scaffold design could be designed to prevent the recurrence of BV by returning vaginal pH below 4.5 and thus preventing the growth of pathogens such as *G. vaginalis*. Next steps include developing printable formulations that incorporate biologics

and evaluating the associated release mechanisms. This study represents a key step towards this goal, focusing on the potential effect of fabrication parameters on active agent release.

REFERENCES

- 1 Bradshaw, C. S. *et al.* High recurrence rates of bacterial vaginosis over the course of 12 months after oral metronidazole therapy and factors associated with recurrence. *J Infect Dis* **193**, 1478-1486, doi:10.1086/503780 (2006).
- 2 Ravel, J., Moreno, I. & Simón, C. Bacterial vaginosis and its association with infertility, endometritis, and pelvic inflammatory disease. *Am J Obstet Gynecol* **224**, 251-257, doi:10.1016/j.ajog.2020.10.019 (2021).
- 3 Fredricks, D. N., Fiedler, T. L. & Marrazzo, J. M. Molecular identification of bacteria associated with bacterial vaginosis. *N Engl J Med* **353**, 1899-1911, doi:10.1056/NEJMoa043802 (2005).
- 4 Sheiness, D., Dix, K., Watanabe, S. & Hillier, S. L. High levels of *Gardnerella vaginalis* detected with an oligonucleotide probe combined with elevated pH as a diagnostic indicator of bacterial vaginosis. *J Clin Microbiol* **30**, 642-648, doi:10.1128/jcm.30.3.642-648.1992 (1992).
- 5 Spiegel, C. A. Bacterial vaginosis. *Clin Microbiol Rev* **4**, 485-502, doi:10.1128/cmr.4.4.485 (1991).
- 6 Czarnobaj, K. & Sawicki, W. The sol-gel prepared SiO₂-CaO-P₂O₅ composites doped with Metronidazole for application in local delivery systems. *Pharm Dev Technol* **17**, 697-704, doi:10.3109/10837450.2011.572894 (2012).
- 7 Paavonen, J. A. & Brunham, R. C. Vaginitis in Nonpregnant Patients: ACOG Practice Bulletin Number 215. *Obstetrics & Gynecology* **135**, 1229-1230, doi:10.1097/aog.0000000000003857 (2020).
- 8 Sharifzadeh, G., Hezaveh, H., Muhamad, II, Hashim, S. & Khairuddin, N. Montmorillonite-based polyacrylamide hydrogel rings for controlled vaginal drug delivery. *Mater Sci Eng C Mater Biol Appl* **110**, 110609, doi:10.1016/j.msec.2019.110609 (2020).
- 9 Verstraete, G. *et al.* Thermoplastic polyurethane-based intravaginal rings for prophylaxis and treatment of (recurrent) bacterial vaginosis. *Int J Pharm* **529**, 218-226, doi:10.1016/j.ijpharm.2017.06.076 (2017).
- 10 Pathak, M., Turner, M., Palmer, C. & Coombes, A. G. Evaluation of polycaprolactone matrices for the intravaginal delivery of metronidazole in the treatment of bacterial vaginosis. *J Biomater Appl* **29**, 354-363, doi:10.1177/0885328214528256 (2014).
- 11 Verstraelen, H., Vervae, C. & Remon, J. P. Rationale and Safety Assessment of a Novel Intravaginal Drug-Delivery System with Sustained DL-Lactic Acid Release, Intended for Long-Term Protection of the Vaginal Microbiome. *PLoS One* **11**, e0153441, doi:10.1371/journal.pone.0153441 (2016).
- 12 Ensign, L. M., Cone, R. & Hanes, J. Nanoparticle-based drug delivery to the vagina: a review. *J Control Release* **190**, 500-514, doi:10.1016/j.jconrel.2014.04.033 (2014).
- 13 Baelo, A. *et al.* Disassembling bacterial extracellular matrix with DNase-coated nanoparticles to enhance antibiotic delivery in biofilm infections. *J Control Release* **209**, 150-158, doi:10.1016/j.jconrel.2015.04.028 (2015).
- 14 Steinbach, J. M. Protein and oligonucleotide delivery systems for vaginal microbicides against viral STIs. *Cell Mol Life Sci* **72**, 469-503, doi:10.1007/s00018-014-1756-3 (2015).
- 15 Sung, Y. K. & Kim, S. W. Recent advances in polymeric drug delivery systems. *Biomaterials Research* **24**, doi:10.1186/s40824-020-00190-7 (2020).
- 16 Rafiei, F. *et al.* Development of Hormonal Intravaginal Rings: Technology and Challenges. *Geburtshilfe Frauenheilkd* **81**, 789-806, doi:10.1055/a-1369-9395 (2021).

- 17 Tighe, B. J. A decade of silicone hydrogel development: surface properties, mechanical properties, and ocular compatibility. *Eye Contact Lens* **39**, 4-12, doi:10.1097/ICL.0b013e318275452b (2013).
- 18 Naumovski, B. & Kapushevska, B. Dimensional Stability and Accuracy of Silicone - Based Impression Materials Using Different Impression Techniques - A Literature Review. *Pril (Makedon Akad Nauk Umet Odd Med Nauki)* **38**, 131-138, doi:10.1515/prilozi-2017-0031 (2017).
- 19 Schubert, C., van Langeveld, M. C. & Donoso, L. A. Innovations in 3D printing: a 3D overview from optics to organs. *Br J Ophthalmol* **98**, 159-161, doi:10.1136/bjophthalmol-2013-304446 (2014).
- 20 Khaled, S. A., Burley, J. C., Alexander, M. R., Yang, J. & Roberts, C. J. 3D printing of tablets containing multiple drugs with defined release profiles. *Int J Pharm* **494**, 643-650, doi:10.1016/j.ijpharm.2015.07.067 (2015).
- 21 Khaled, S. A., Burley, J. C., Alexander, M. R., Yang, J. & Roberts, C. J. 3D printing of five-in-one dose combination polypill with defined immediate and sustained release profiles. *J Control Release* **217**, 308-314, doi:10.1016/j.jconrel.2015.09.028 (2015).
- 22 Fu, J., Yu, X. & Jin, Y. 3D printing of vaginal rings with personalized shapes for controlled release of progesterone. *Int J Pharm* **539**, 75-82, doi:10.1016/j.ijpharm.2018.01.036 (2018).
- 23 Tiboni, M., Campana, R., Frangipani, E. & Casettari, L. 3D printed clotrimazole intravaginal ring for the treatment of recurrent vaginal candidiasis. *Int J Pharm* **596**, 120290, doi:10.1016/j.ijpharm.2021.120290 (2021).
- 24 Elkasabgy, N. A., Mahmoud, A. A. & Maged, A. 3D printing: An appealing route for customized drug delivery systems. *Int J Pharm* **588**, 119732, doi:10.1016/j.ijpharm.2020.119732 (2020).
- 25 Januszewicz, R., Mecham, S. J., Olson, K. R. & Benhabbour, S. R. Design and Characterization of a Novel Series of Geometrically Complex Intravaginal Rings with Digital Light Synthesis. *Adv Mater Technol* **5**, doi:10.1002/admt.202000261 (2020).
- 26 Sethi, R. *et al.* Clinical applications of custom-made vaginal cylinders constructed using three-dimensional printing technology. *J Contemp Brachytherapy* **8**, 208-214, doi:10.5114/jcb.2016.60679 (2016).
- 27 Hou, C. *et al.* Printing 3D vagina tissue analogues with vagina decellularized extracellular matrix bioink. *Int J Biol Macromol* **180**, 177-186, doi:10.1016/j.ijbiomac.2021.03.070 (2021).
- 28 Asnaashari, S., Khoei, N. S., Zarrintan, M. H., Adibkia, K. & Javadzadeh, Y. Preparation and evaluation of novel metronidazole sustained release and floating matrix tablets. *Pharm Dev Technol* **16**, 400-407, doi:10.3109/10837451003774393 (2011).
- 29 Owen, D. H. & Katz, D. F. A vaginal fluid simulant. *Contraception* **59**, 91-95, doi:10.1016/s0010-7824(99)00010-4 (1999).
- 30 Tietz, K. & Klein, S. Simulated Genital Tract Fluids and Their Applicability in Drug Release/Dissolution Testing of Vaginal Dosage Forms. *Dissolution Technologies* **25**, 40-51, doi:10.14227/dt250318p40 (2018).
- 31 Liu, X., Champagne, C. P., Lee, B. H., Boye, J. I. & Casgrain, M. Thermostability of Probiotics and Their alpha -Galactosidases and the Potential for Bean Products. *Biotechnol Res Int* **2014**, 472723, doi:10.1155/2014/472723 (2014).
- 32 Hua, Y. *et al.* Improving the Thermostability of Glutamate Decarboxylase from *Lactobacillus brevis* by Consensus Mutagenesis. *Appl Biochem Biotechnol* **191**, 1456-1469, doi:10.1007/s12010-020-03283-0 (2020).
- 33 Petrina, M. A. B., Cosentino, L. A., Rabe, L. K. & Hillier, S. L. Susceptibility of bacterial vaginosis (BV)-associated bacteria to secnidazole compared to metronidazole, tinidazole and clindamycin. *Anaerobe* **47**, 115-119, doi:10.1016/j.anaerobe.2017.05.005 (2017).

- 34 Alauzet, C., Lozniewski, A. & Marchandin, H. Metronidazole resistance and nim genes in anaerobes: A review. *Anaerobe* **55**, 40-53, doi:10.1016/j.anaerobe.2018.10.004 (2019).
- 35 Austin, M. N., Beigi, R. H., Meyn, L. A. & Hillier, S. L. Microbiologic response to treatment of bacterial vaginosis with topical clindamycin or metronidazole. *J Clin Microbiol* **43**, 4492-4497, doi:10.1128/jcm.43.9.4492-4497.2005 (2005).
- 36 Thulkar, J., Kriplani, A. & Agarwal, N. A comparative study of oral single dose of metronidazole, tinidazole, secnidazole and ornidazole in bacterial vaginosis. *Indian J Pharmacol* **44**, 243-245, doi:10.4103/0253-7613.93859 (2012).
- 37 Li, T. *et al.* Antimicrobial Susceptibility Testing of Metronidazole and Clindamycin against Gardnerella vaginalis in Planktonic and Biofilm Formation. *Can J Infect Dis Med Microbiol* **2020**, 1361825, doi:10.1155/2020/1361825 (2020).
- 38 Tosun, I. *et al.* [Biotypes and antibiotic resistance patterns of Gardnerella vaginalis strains isolated from healthy women and women with bacterial vaginosis]. *Mikrobiyol Bul* **41**, 21-27 (2007).
- 39 Jones, B. M., Geary, I., Alawattagama, A. B., Kinghorn, G. R. & Duerden, B. I. In-vitro and in-vivo activity of metronidazole against Gardnerella vaginalis, Bacteroides spp. and Mobiluncus spp. in bacterial vaginosis. *J Antimicrob Chemother* **16**, 189-197, doi:10.1093/jac/16.2.189 (1985).
- 40 Dash, S., Murthy, P. N., Nath, L. & Chowdhury, P. Kinetic modeling on drug release from controlled drug delivery systems. *Acta Pol Pharm* **67**, 217-223 (2010).
- 41 Higuchi, T. MECHANISM OF SUSTAINED-ACTION MEDICATION. THEORETICAL ANALYSIS OF RATE OF RELEASE OF SOLID DRUGS DISPERSED IN SOLID MATRICES. *J Pharm Sci* **52**, 1145-1149, doi:10.1002/jps.2600521210 (1963).
- 42 Costa, P. & Sousa Lobo, J. M. Modeling and comparison of dissolution profiles. *Eur J Pharm Sci* **13**, 123-133, doi:10.1016/s0928-0987(01)00095-1 (2001).
- 43 Peppas, N. A. & Sahlin, J. J. A simple equation for the description of solute release. III. Coupling of diffusion and relaxation. *International Journal of Pharmaceutics* **57**, 169 (1989).
- 44 Clark, J. T. *et al.* Quantitative evaluation of a hydrophilic matrix intravaginal ring for the sustained delivery of tenofovir. *J Control Release* **163**, 240-248, doi:10.1016/j.jconrel.2012.08.033 (2012).
- 45 Johnson, T. J., Gupta, K. M., Fabian, J., Albright, T. H. & Kiser, P. F. Segmented polyurethane intravaginal rings for the sustained combined delivery of antiretroviral agents dapivirine and tenofovir. *European Journal of Pharmaceutical Sciences* **39**, 203-212, doi:10.1016/j.ejps.2009.11.007 (2010).
- 46 Barnhart, K. T., Timbers, K., Pretorius, E. S., Lin, K. & Shaunik, A. In vivo assessment of NuvaRing placement. *Contraception* **72**, 196-199, doi:10.1016/j.contraception.2005.03.012 (2005).
- 47 Latha, S. *et al.* Formulation development and evaluation of metronidazole magnetic nanosuspension as a magnetic-targeted and polymeric-controlled drug delivery system. *Journal of Magnetism and Magnetic Materials* **321**, 1580-1585 (2009).
- 48 Ozyazici, M., Gökçe, E. H. & Ertan, G. Release and diffusional modeling of metronidazole lipid matrices. *Eur J Pharm Biopharm* **63**, 331-339, doi:10.1016/j.ejpb.2006.02.005 (2006).
- 49 Wróblewska, M., Szymańska, E., Szekalska, M. & Winnicka, K. Different Types of Gel Carriers as Metronidazole Delivery Systems to the Oral Mucosa. *Polymers (Basel)* **12**, doi:10.3390/polym12030680 (2020).
- 50 Forbes, C. J. *et al.* Non-aqueous silicone elastomer gels as a vaginal microbicide delivery system for the HIV-1 entry inhibitor maraviroc. *J Control Release* **156**, 161-169, doi:10.1016/j.jconrel.2011.08.006 (2011).

- 51 Javadzadeh, Y. *et al.* Evaluation of drug release kinetics and physico-chemical characteristics of metronidazole floating beads based on calcium silicate and gas-forming agents. *Pharm Dev Technol* **15**, 329-338, doi:10.3109/10837450903196843 (2010).
- 52 Snorradóttir, B. S., Jónsdóttir, F., Sigurdsson, S. T., Thorsteinsson, F. & Másson, M. Numerical modelling and experimental investigation of drug release from layered silicone matrix systems. *Eur J Pharm Sci* **49**, 671-678, doi:10.1016/j.ejps.2013.05.006 (2013).
- 53 Krenzlin, S. *et al.* Predictability of drug release from cochlear implants. *J Control Release* **159**, 60-68, doi:10.1016/j.jconrel.2011.12.032 (2012).
- 54 Calija, B. *et al.* An investigation of formulation factors affecting feasibility of alginate-chitosan microparticles for oral delivery of naproxen. *Arch Pharm Res* **34**, 919-929, doi:10.1007/s12272-011-0609-y (2011).
- 55 Fraser, I. S. *et al.* Vaginal epithelial surface appearances in women using vaginal rings for contraception. *Contraception* **61**, 131-138, doi:10.1016/s0010-7824(00)00081-0 (2000).
- 56 Weisberg, E. *et al.* A randomized comparison of the effects on vaginal and cervical epithelium of a placebo vaginal ring with non-use of a ring. *Contraception* **62**, 83-89, doi:10.1016/s0010-7824(00)00137-2 (2000).
- 57 Kim, J. H. Urogynecology and Reconstructive Pelvic Surgery. 4th ed. *Int Neurourol J* **19**, 51, doi:10.5213/inj.2015.19.1.51 (2015).
- 58 Eberhart, R., Chuong, C. J. & Zimmern, P. Exploring biomechanical methods to study the human vaginal wall. *Neurourol Urodyn* **36**, 499-506, doi:10.1002/nau.22968 (2017).

APPENDIX

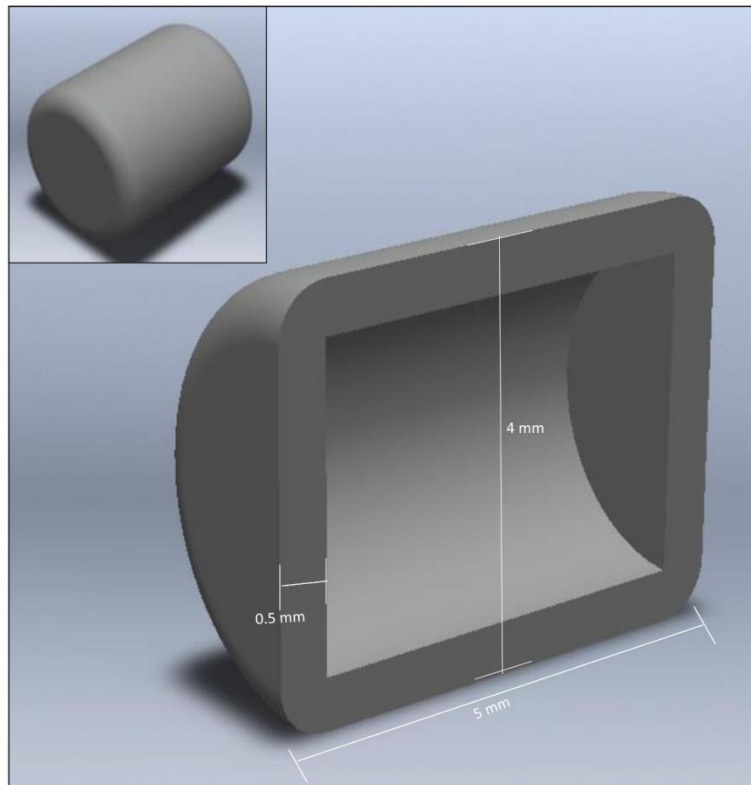


FIGURE 1 - Cross-sectional and isometric view of tested 3D-printed scaffold design.

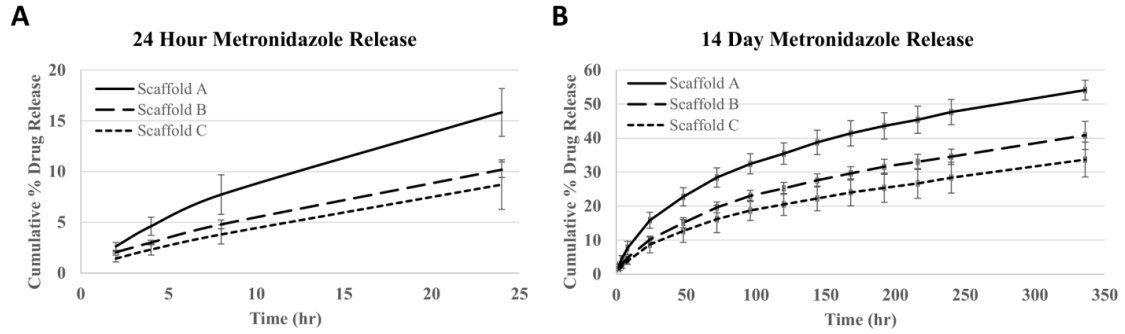


FIGURE 2 - Metronidazole release from 3D printed scaffolds using three replicates. (A) Short-term release over 24 hr. (B) Long-term release over 14 d. After 24 hr (Scaffold B and C: $p \leq 0.05$) and 14 d (Scaffold B, C: $p \leq 0.05$; $p \leq 0.01$), Scaffold A had higher release than Scaffold B and C; release from Scaffolds B and C were similar ($p > 0.05$). Error bars represent standard deviation.

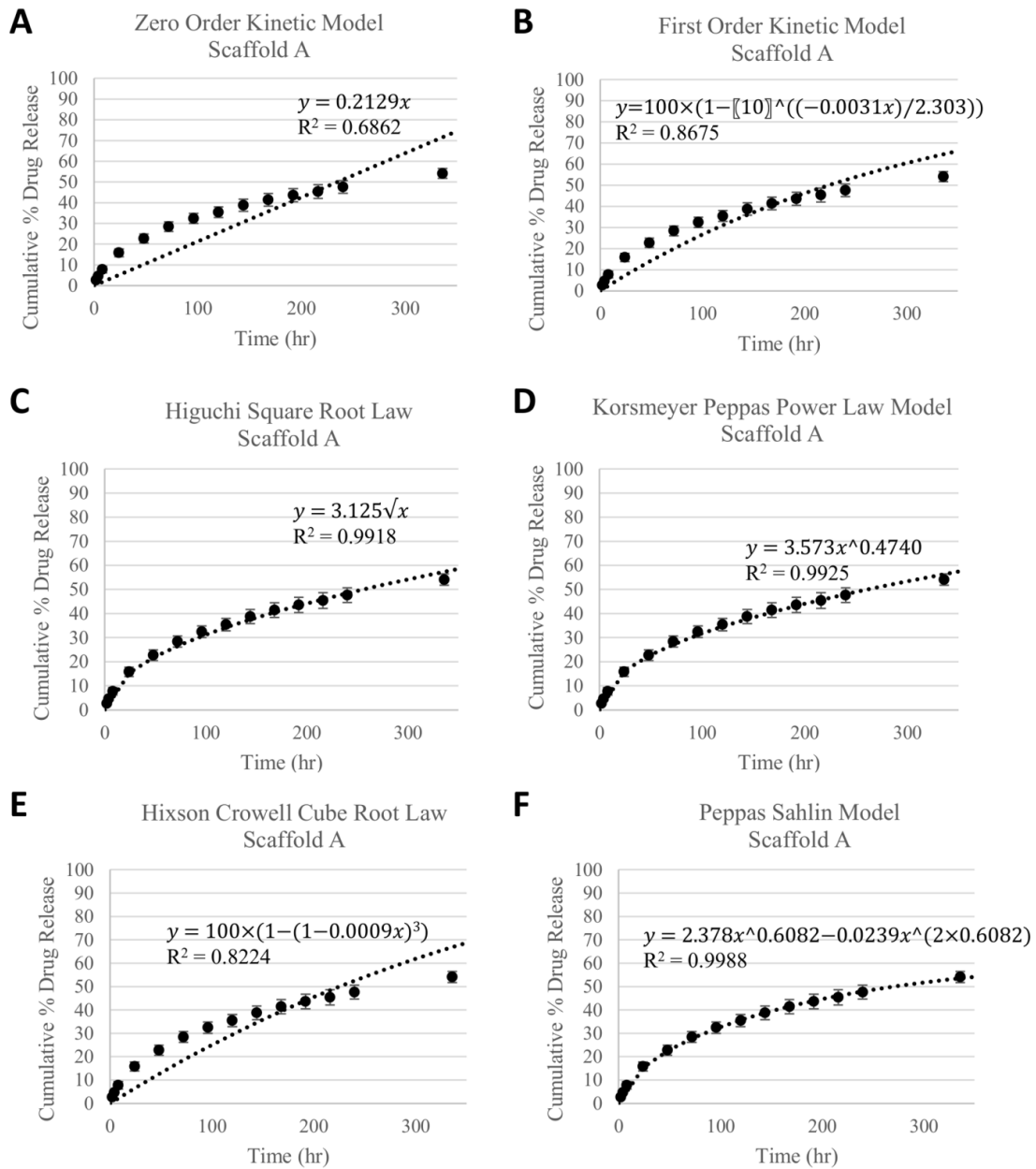


FIGURE 3 - Metronidazole release from Scaffold A fitted to A) Zero order kinetic, B) First order kinetic, C) Higuchi, D) Korsmeyer-Peppas, E) Hixson Crowell, and F) Peppas-Sahlin models. The equation of best fit line and R^2 values, representing the adequacy of the fit, are shown on each plot.

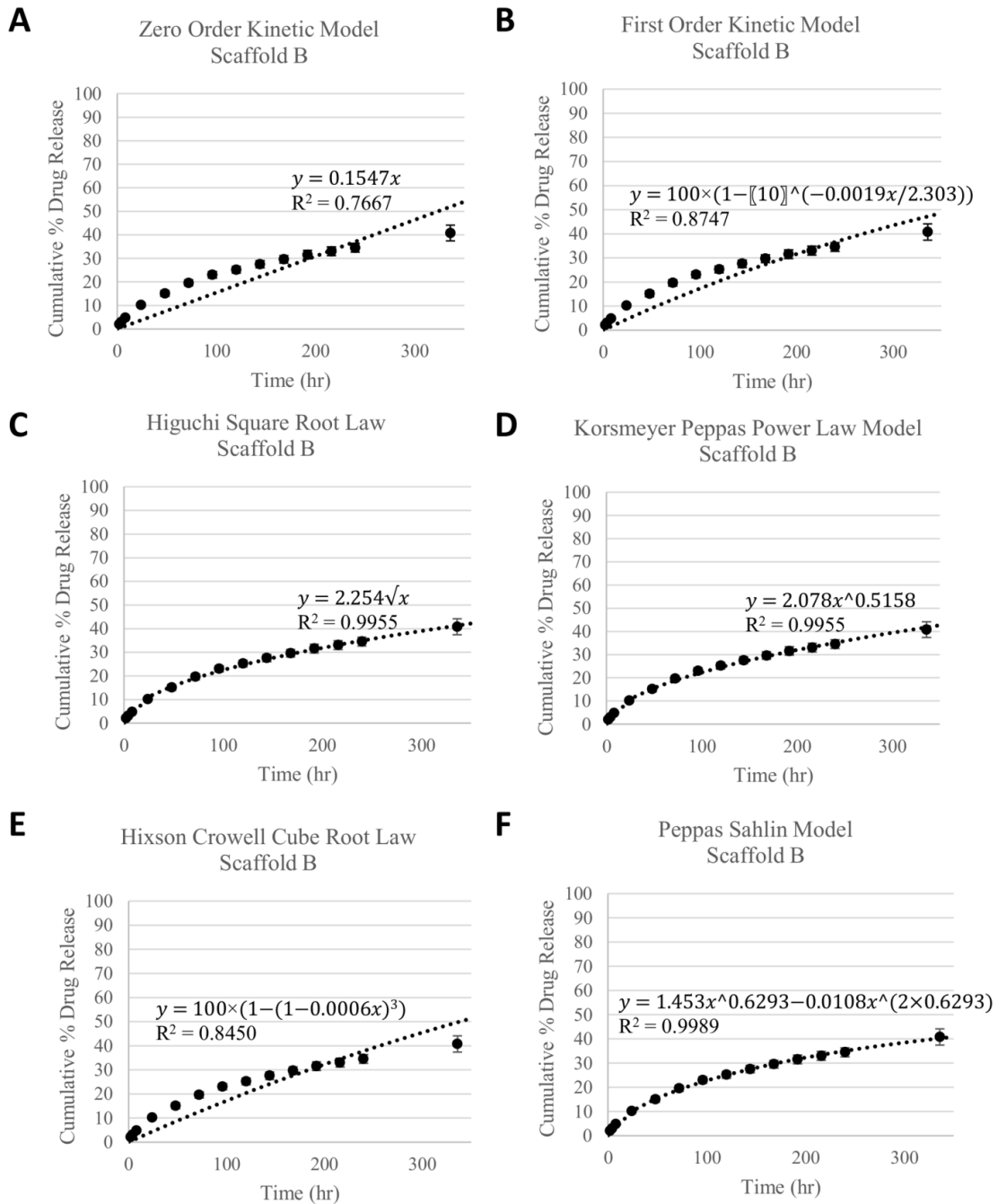


FIGURE 4 - Metronidazole release from Scaffold B fitted to A) Zero order kinetic, B) First order kinetic, C) Higuchi, D) Korsmeyer-Peppas, E) Hixson Crowell, and F) Peppas-Sahlin models. The equation of best fit line and R^2 values, representing the adequacy of the fit, are shown on each plot.

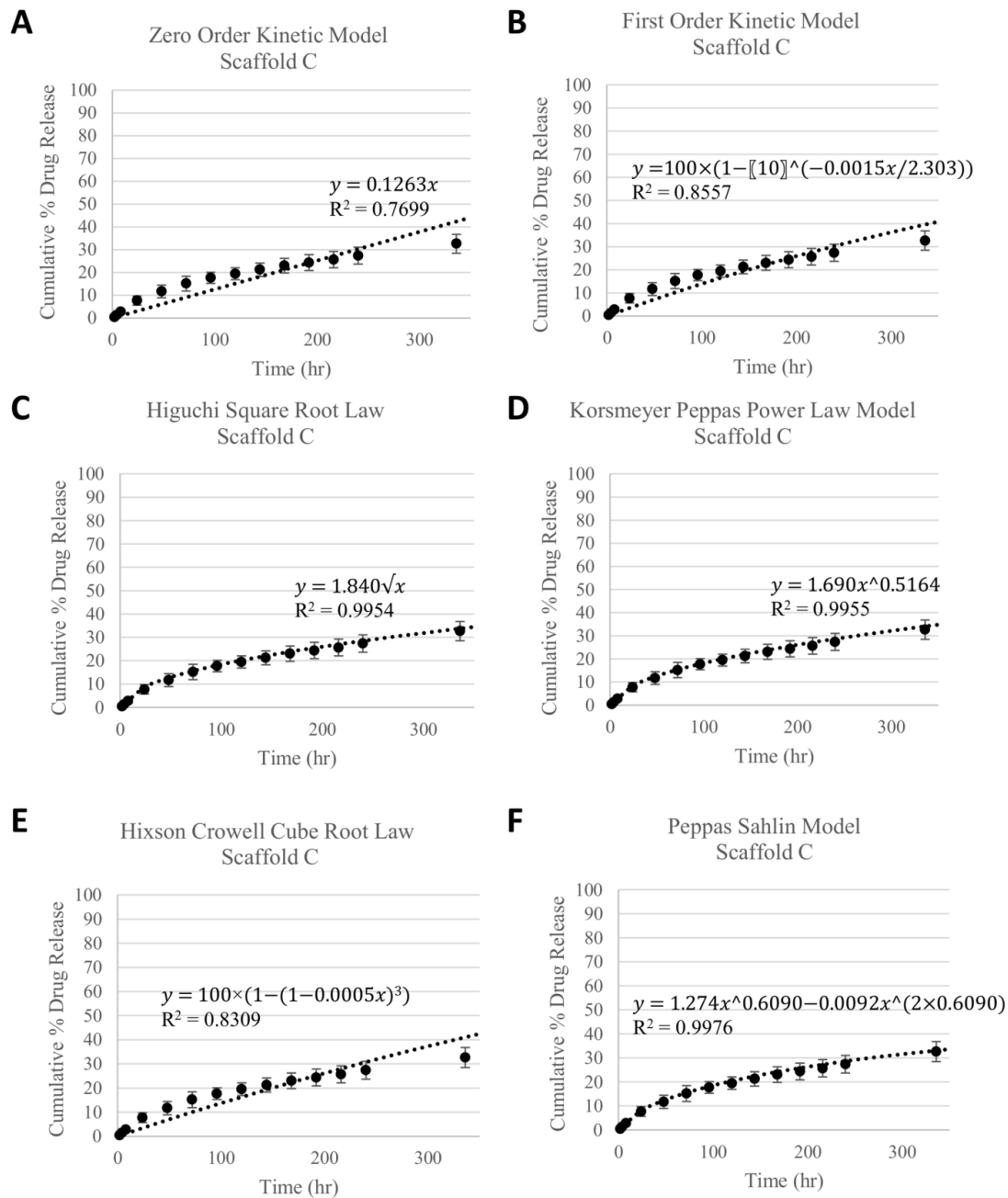


FIGURE 5 - Metronidazole release from Scaffold C fitted to A) Zero Order kinetic, B) First Order kinetic, C) Higuchi, D) Korsmeyer-Peppas, E) Hixson Crowell, and F) Peppas-Sahlin models. The equation of best fit line and R^2 values, representing the adequacy of the fit, is shown on each plot.

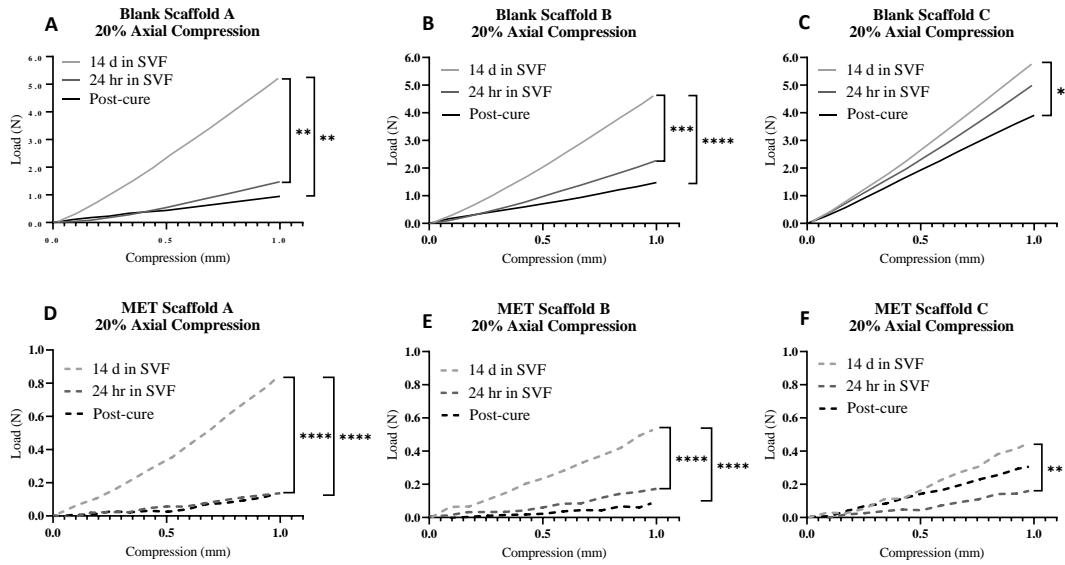


FIGURE 6 - Blank silicone and metronidazole-containing scaffolds were evaluated under 20% axial compression as a function of curing condition (Scaffolds A, B, and C), immediately post-cure and after 24 hr and 14 d in SVF. Load is shown as a function of axial compression of (A-C) blank scaffolds A, B, and C and (D-F) metronidazole-containing scaffolds A, B, and C. Mechanical testing was performed using five replicates per curing condition. Statistical significance between experimental groups, as calculated by one-way ANOVA, is represented by * $p \leq 0.05$, ** $p \leq 0.01$, *** $p \leq 0.001$, **** $p \leq 0.0001$. Please note y-axes scale differences between blank and metronidazole-containing scaffolds.

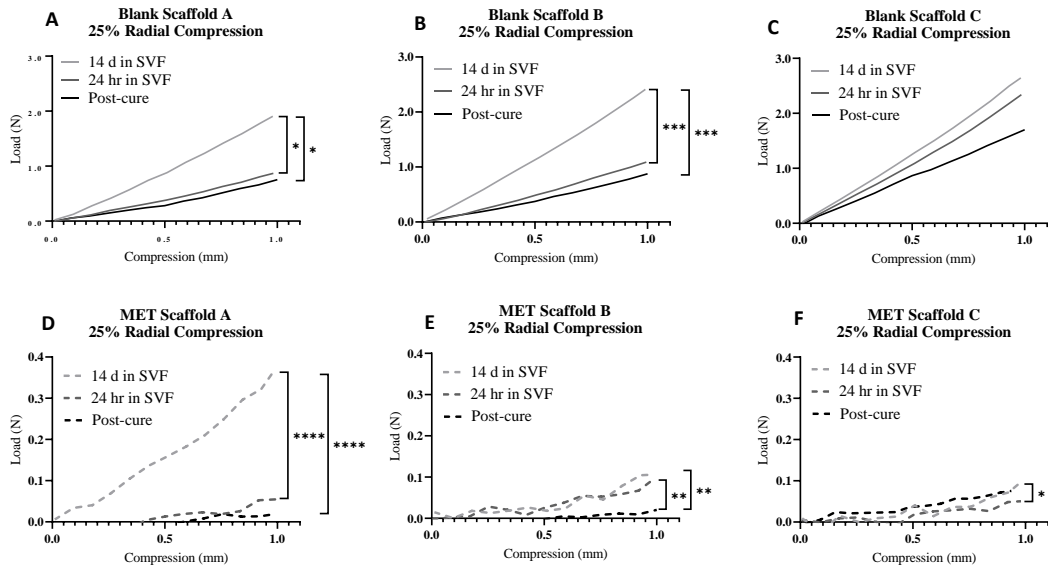


FIGURE 7 - Blank silicone and metronidazole-containing scaffolds were evaluated under 25% radial compression as a function of curing condition (Scaffolds A, B, and C), immediately post-cure and after 24 hr and 14 d in SVF. Load is shown as a function of radial compression of (A-C) blank scaffolds A, B, and C and (D-F) metronidazole-containing scaffolds A, B, and C. Mechanical testing was performed using five replicates per curing condition. Statistical significance between experimental groups, as calculated by one-way ANOVA, is represented by * $p \leq 0.05$, ** $p \leq 0.01$, *** $p \leq 0.001$, **** $p \leq 0.0001$. Please note y-axes scale differences between blank and metronidazole-containing scaffolds.

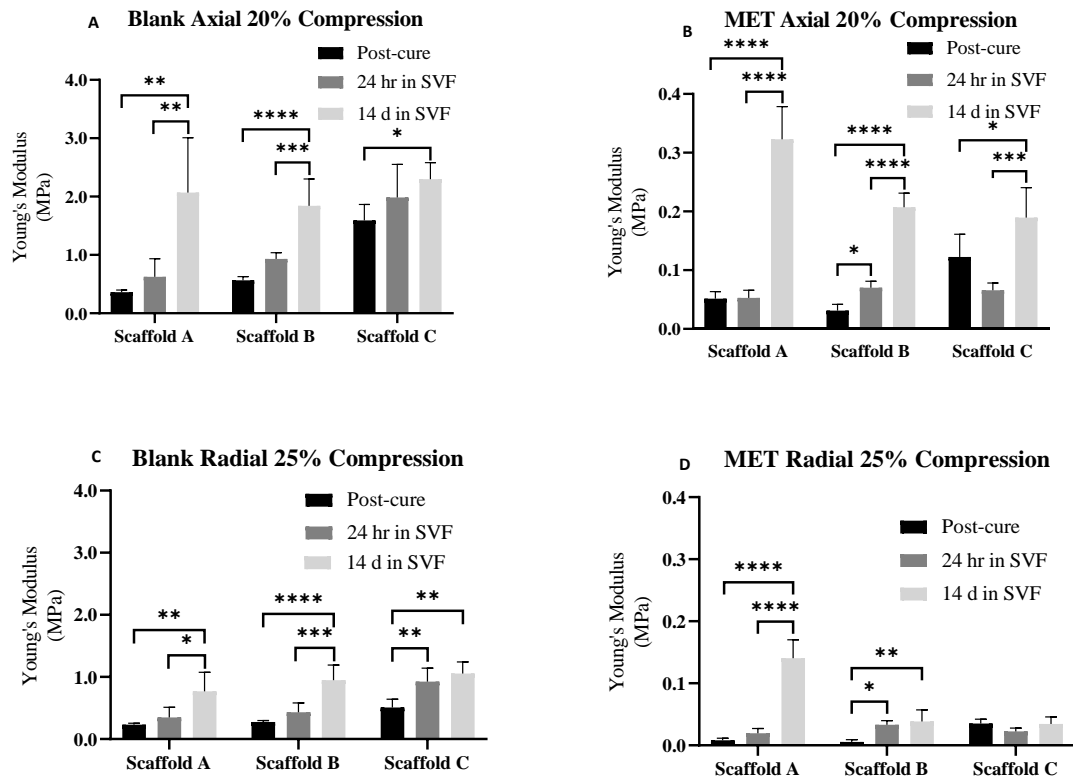


FIGURE 8 - Young's modulus of (A) blank and (B) metronidazole-containing scaffolds compressed by 20% in the axial direction and (C) blank and (D) metronidazole-containing scaffolds compressed by 25% in the radial direction. Mechanical testing was performed using five replicates per curing condition. Statistical significance between experimental groups, as calculated by one-way ANOVA, is represented by * $p \leq 0.05$, ** $p \leq 0.01$, *** $p \leq 0.001$, **** $p \leq 0.0001$. Please note y-axes scale differences between blank (A, C) and metronidazole-containing (B, D) scaffolds.

TABLE I
CORRELATION VALUES AND RATE CONSTANTS OF EACH MODEL FOR
SCAFFOLDS A, B, AND C.

Model	Scaffold		
	A	B	C
Zero Order Kinetic Model	k = 0.2129 R ² = 0.6862	k = 0.1547 R ² = 0.7667	k = 0.1263 R ² = 0.7699
First Order Kinetic Model	k = 0.0023 R ² = 0.9438	k = 0.0015 R ² = 0.9494	k = 0.0012 R ² = 0.9442
Higuchi Square Root Model	k = 3.125 R ² = 0.9918	k = 2.254 R ² = 0.9955	k = 1.840 R ² = 0.9954
Korsmeyer-Peppas Model	k = 3.573 n = 0.4740 R ² = 0.9931	k = 2.078 n = 0.5158 R ² = 0.9959	k = 1.690 n = 0.5164 R ² = 0.9958
Peppas-Sahlin Model	k _d = 2.378 k _r = -0.2390 m = 0.6082 R ² = 0.9990	k _d = 1.453 k _r = -0.0107 m = 0.6293 R ² = 0.9990	k _d = 1.274 k _r = -0.0091 m = 0.6090 R ² = 0.9980
Hixson-Crowell Model	k = 0.0009 R ² = 0.8224	k = 0.0006 R ² = 0.8450	k = 0.0005 R ² = 0.8304

CURRICULUM VITA

NAME: Sydney Elizabeth Herold

ADDRESS: Department of Bioengineering
220 Eastern Parkway
University of Louisville
Louisville, KY 40292

DOB: April 21, 1999

EDUCATION & TRAINING: B.S., Bioengineering
University of Louisville
2017-2021

M.Eng., Bioengineering
University of Louisville
2021-2022

AWARDS:

PROFESSIONAL SOCIETIES:

PUBLICATIONS:

NATIONAL MEETING
PRESENTATIONS:

REFEREED JOURNALS:

BOOKS AND SYMPOSIA:

INVITED PRESENTATIONS: